Improved thermography technique for identifying structural elements under ambient conditions

K. Sivasubramanian[1,*], K. P. Jaya[2] and K. Ramanjaneyulu[1]

[1]CSIR-Structural Engineering Research Centre, Taramani, Chennai 600 113, India
[2]Structural Engineering Division, Department of Civil Engineering, Anna University, CEG Campus, Chennai 600 025, India

Infrared thermography is an interesting non-contact evaluation technique which relies on surface thermal gradient. It is used to identify dissimilarity in geometry or material property. The application of this method in civil engineering is limited, as concrete components are heavy and require large amount of heat to reveal differential thermal gradients. Hence, the present work focuses on assessing the applicability of the infrared thermography technique for civil engineering structures under ambient conditions using solar heat. For the study, the exterior frames in real structures have been chosen, wherein the reinforced concrete and masonry members are not explicitly visible to the eye. The initial studies showed that the thermograms revealed different temperature gradients corresponding to the main beams and masonry walls, thus aiding in their identification. However, when the method was extended to multi-storey framed structures, the thinner elements like lintel beams could not be identified. The application of improved thermography technique using wavelet packet analysis to two test structures showed that lintel beams could also be identified. Also, the possibility to evaluate the geometric dimensions of structural members and floor heights, using the thermogram and a reference dimension, has been studied on two test structures. The geometric dimensions could be evaluated with more than 90% accuracy.

Keywords: Brick masonry, concrete, infrared thermography, structural element, wavelet packets.

INFRARED thermography is a fast-growing research field. Thermography has found applications in swine flu detection; cancer diagnosis[1]; overheating of circuit boards, transformers and study of equipment reliability[1,2]; and monitoring molten slag in iron and steel factories[3,4]. These applications of thermography rely on the ability of the object under diagnosis to emit infrared (IR) rays because of the inherent heat in the test medium. In all these cases, as no external heat source is required, the IR camera alone is sufficient to perform the study and is called passive thermography.

However, the evaluation of composites in aerospace industry[5–7] uses active infrared thermography (IRT). In the active type IRT, filtered incandescent source or IR diode illuminator or filtered xenon flash is used to pulse heat energy into the test object for a short period of time. The composite components which are thinner have been found to respond to the thermal pulse and thus yield differential thermal gradients if delaminations/defects are present.

The applicability of IRT to concrete and masonry structures is constrained by the fact that they do not possess inherent heat flow. This implies that an external heating source needs to be employed. The massive size of the structural elements in civil engineering demands much stronger heating than that available from the IR flash lamps. The IR flash lamp being popularly used as a heating source in aerospace engineering, could not be used for concrete and masonry structures because of their lower heat intensity.

In concrete structures, IRT is being popularly employed for detection of shallow depth delamination[8,9]. Further, research on the applicability of IRT for civil engineering applications is being pursued[10]. Research in the recent past has led to the detection of defects in pavements[11], embankment deterioration[12] and non-destructive testing in concrete[13,14]. However, in India, limited research or application of this method has been observed from the literature.

In the present work, ambient solar heat has been used to identify and differentiate between the concrete and masonry elements. The present work focuses on the exterior frames of the reinforced concrete (RC) structures for identifying these elements. Especially in a growing field like the IRT technique, the application of numerical techniques to improve the results is always appreciable. Also, many-a-times, the available commercial package might not be in a position to provide satisfactory results. The present work focuses on applying the wavelet packets for denoising and improving the thermograms captured using the IR camera. It is proposed to identify the location of

*For correspondence. (e-mail: ksiva@serc.res.in)

smaller elements like lintel beams which are not explicitly visible in the IR thermogram.

Infrared thermography

IRT relies on infrared rays emitted by the test object to develop the thermograms. William Herschel discovered the presence of IR rays in visible light in 1800. Only in 1830, the first detectors were developed for IR rays. IRT is based on the principle that all bodies, above absolute zero temperature (0 K), emit heat/thermal infrared radiations. It has also been observed that the intensity of this radiation depends on the wavelength and temperature of the body[15]. Subsequently, the focus of research shifted towards the development on IR detectors till the mid-1900s. With the development of better IR detectors, the thermography technique gained popularity for various applications.

Here, the Planck's law is used to evaluate the radiance of heat from a blackbody, and its inverse is used to evaluate the temperature on a blackbody. Later, Wien's law and Stefan–Boltzmann law have strengthened the thermography method in evaluating the temperature on the body surface[15]. The thermography method uses a camera capable of detecting the radiations/rays in the IR zone.

The VarioCam® HR RESEARCH 600 camera has been used in the present work (Figure 1). It is an uncooled IRT camera with temperature sensitivity of 0.03 K at 30°C. The camera has a graphic resolution of 1280 × 960 pixels. IR cameras with the best temperature sensitivity and graphic resolution are now preferred for research applications. While the temperature sensitivity plays an important role in enabling the visualization of subtle changes in the temperature of the test object, the graphic resolution is important in providing clarity in the thermogram image.

The IRT camera resembles a camcorder, but detects variations in IR emission and displays them as thermal gradients in real-time. This camera feature is being used in thermography method. It needs to be mentioned here that the IRT method is a non-contact method which makes it possible to conduct the evaluation process at a distance from the test object. Also, the IRT method does not involve the use of any radiations harmful to the operator. It only uses the radiations from the test object for the evaluation. Hence, this technique is harmless to use.

Many-a-times the collected raw signals need to be filtered to remove the noisy components. This helps in improved interpretation of the results. In the present work, it is proposed to apply the wavelet packet analysis to improve the IR thermograms with the aim of obtaining more details about the structural elements.

Wavelet packets analysis

Wavelet packet is a type of wavelet transform. Wavelet transform is a signal processing technique being popularly used for filtering unwanted frequencies in the signal[16–18]. Wavelet transform has found applications in several engineering disciplines. It is being popularly used in several applications like the construction of JPEG2000 images, data compression and noise reduction[19], edge detection in images and in structural applications for system identification[20], nonlinear analysis[21], earthquake analysis[22,23], analysing bridges[24], smart structures[25,26], vibration control[27], damage identification[28–34], fire damaged structures[35] and many other structural applications.

In the earlier research works[28–31], the need was to segregate the high frequency content from the low frequency counterparts, to identify the location of damage. A one-level analysis using discrete or continuous wavelet transforms was used. In the present work, the powerful wavelet packets have been used. The wavelet packet analysis is preferred over the other types of wavelet transform when the signal contains closely placed frequencies. With wavelet packets, it is possible to eliminate narrow range noisy frequency bands.

Figure 1. Infrared thermography equipment. ***a***, IR camera; ***b***, Camera and processing laptop.

The 1D wavelet transform produces two components when applied to a signal as shown in Figure 2. In other words, the wavelet filter bank uses a low-pass and high-pass filter to produce two components (Figure 3 *a*). The inverse transform is used to reconstruct the signal using the approximations (Figure 3 *b*).

The mother wavelet forms the basis of the wavelet analysis. The mother wavelet is a waveform that has limited duration and an average value of zero. Based on this mother wavelet, the wavelet kernel can be expressed by

$$\psi_{a,b}(t) = \frac{1}{\sqrt{|a|}}\psi\left(\frac{t-b}{a}\right), \tag{1}$$

where t is the time and a and b are real. Here, the scale and translation parameters (j and k) are chosen based on powers of two, and there exists $\psi(t)$ with good time–frequency localization property. The set of functions $\psi(t)$ is denoted as:

$$\psi_{j,k}(t) = 2^{j/2}\psi(2^j t - k), \tag{2}$$

which constitutes an orthonormal basis for $L^2(\Re)$. Here j and k are integers and $L^2(\Re)$ denotes the class of measurable square-integrable function $x(t)$ in $\Re$. Any signal $x(t)$ in $L^2(\Re)$ can be expressed as a sum over j, k of the product of (the inner product of f and $\psi_{j,k}$) and $\psi_{j,k}(t)$ expressed as:

$$x(t) = \sum_{j,k}\langle f, \psi_{j,k}\rangle \psi_{j,k}(t), \tag{3}$$

This is called the discrete wavelet transform (DWT). In wavelet transform analysis, one of the important characteristics which help in selection of a particular wavelet for a problem is the number of vanishing moments of the wavelet. The nth moment of a function $\psi(t)$ is represented by $\int_{-\infty}^{\infty} t^n \psi(t)\mathrm{d}t$. When $m+1$ moments of the wavelet are zero, $\int_{-\infty}^{\infty} t^n \psi(t)\mathrm{d}t = 0$ for $n = 0, \ldots, m$, then the number of vanishing moments of the wavelet is m. When a wavelet has m vanishing moments, suppression of signals that are polynomials of a degree lower than or equal to m is ensured. In other words, if a wavelet is m times differentiable, the wavelet has at least m vanishing moments.

Wavelet packet analysis employs multiple decomposition of approximations and details to many levels. That is, it involves the application of the one-dimensional wavelet transforms several times in a procedural manner. This empowers the user to exercise better control on filtering the noise. The wavelet packet analysis is schematically represented in Figure 4. The processing of signals using wavelet transforms requires the selection of the appropriate mother wavelet from the several available functions. The effectiveness of the mother wavelet function for a particular problem is dependent on the identification of its number of vanishing moments. Studies have been carried out to identify these parameters and routines have been developed using Matlab® software to enhance the thermograms.

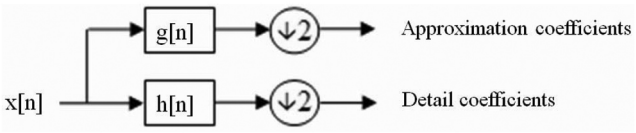

Figure 2. Schematic of the wavelet transform and its components.

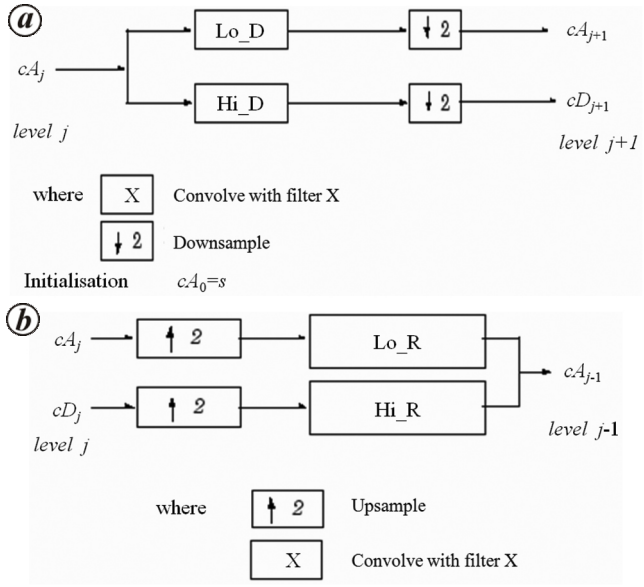

Figure 3. Schematic of the decomposition (***a***) and reconstruction (***b***) in 1D wavelet transform.

Experimental studies

Studies using infrared thermography

The first test structure (TS1) is a simple structure with masonry walls and RC beam-cum-slab on the roof. The structure houses the water pump for a laboratory. The experiment has been carried out under ambient heating at noon. The maximum day temperature recorded on that day was 30°C. IRT method has been applied to identify the differential emissivity from different materials, namely masonry and reinforced concrete. Figure 5 shows the test structure and its thermogram. As masonry and concrete have different heat absorption and emission characteristics, over a period of time they have been observed to reach different temperatures. This results in different levels of IR emission from the two materials. Hence, the thermogram clearly shows the masonry and RC structural elements in different colours.

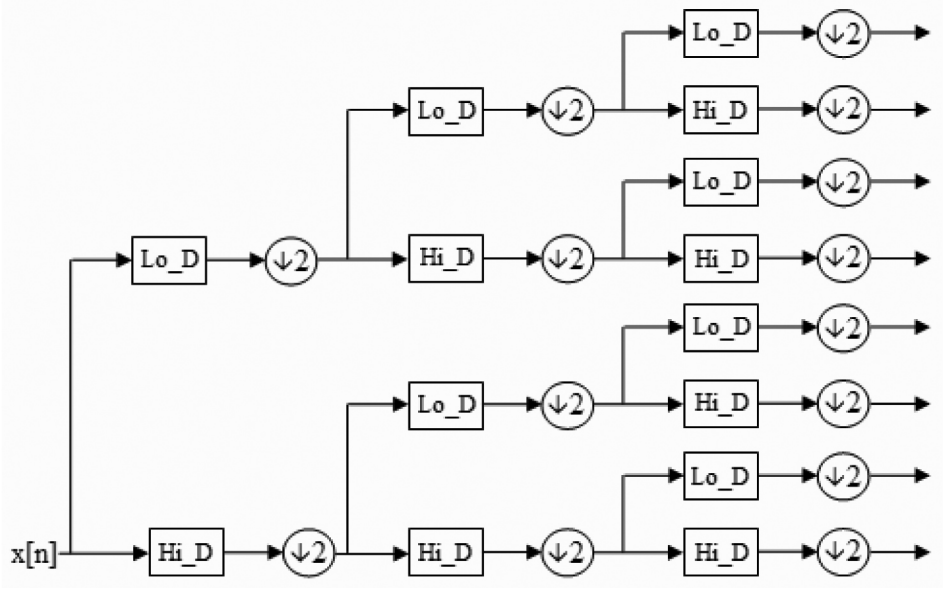

Figure 4. Schematic of the wavelet packet analysis.

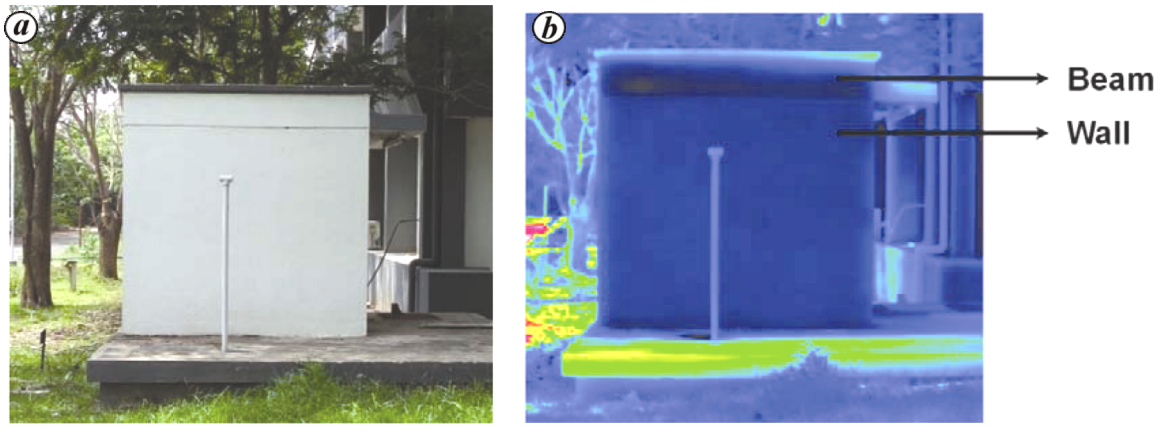

Figure 5. Thermogram of a pump house building (TS1). ***a***, Test structure 1; ***b***, Thermogram.

In the second case, a laboratory shed structure (TS2) has been studied. The exterior frame of the structure has been studied for RC columns, beams, purlin and masonry infill. In this case, even though a clear view could not be obtained because of the presence of trees in the proximity, it has still been possible to identify the structural members from the thermogram. The photograph of the structure and the thermogram are shown in Figure 6 *a* and *b* respectively. The identified structural elements are highlighted for better understanding in the thermogram (Figure 6 *b*). To improve the understanding, two more test structures (TS3 and TS4 respectively) have been studied. The structural elements identified from the thermogram are indicated for better clarity. The thermogram of TS3 and TS4 are shown in Figures 7 and 8 respectively.

In all these cases, IRT has been used to identify the masonry wall and the RC beams. These case studies have been demonstrated under ambient solar heat. It may be noticed here that the heat energy used in this case is much higher than that produced in active thermography flash lamps. Thus, it can be observed that even with sustained mild heating (obtained from ambient conditions), it is possible to identify structural elements with different material properties. But, when the same procedure was extended to multi-storey framed structures, difficulties arose in identifying the smaller RC members like lintel beams. Hence, it is proposed to apply denoising and enhance the details that could be obtained from the thermogram.

Studies using improved infrared thermography

The improved thermography technique uses the wavelet packets for the processing and enhancement of the results from the IR thermogram. By applying improved signal processing techniques, the less trivial details are enhanced and it is expected to improve the non-destructive

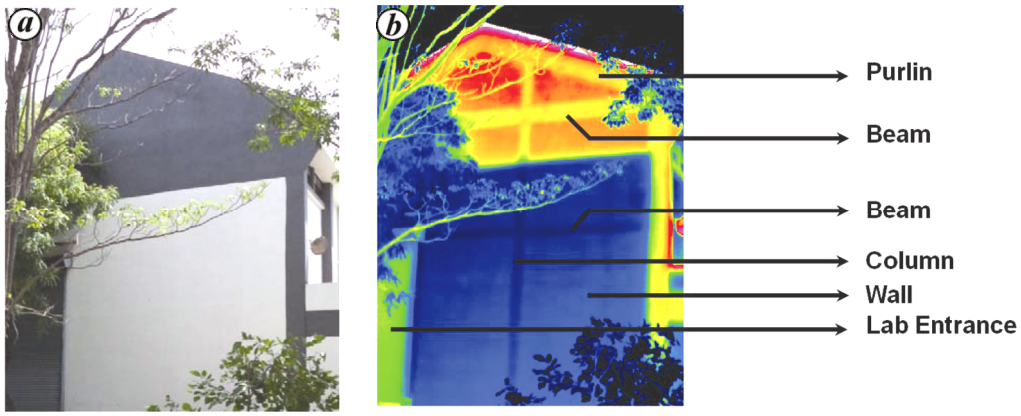

Figure 6. Thermogram of a laboratory shed building (TS2). ***a***, Test structure 2; ***b***, Thermogram.

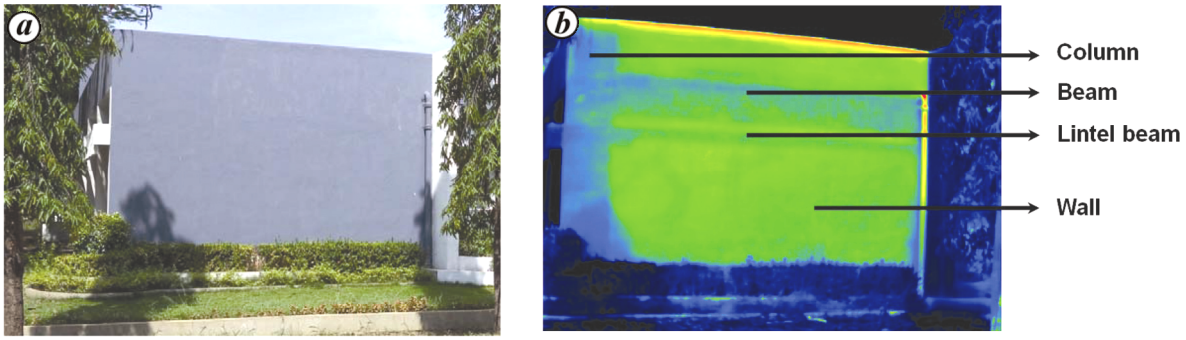

Figure 7. Structural element identification on structure TS3. ***a***, Test structure 3; ***b***, Thermogram.

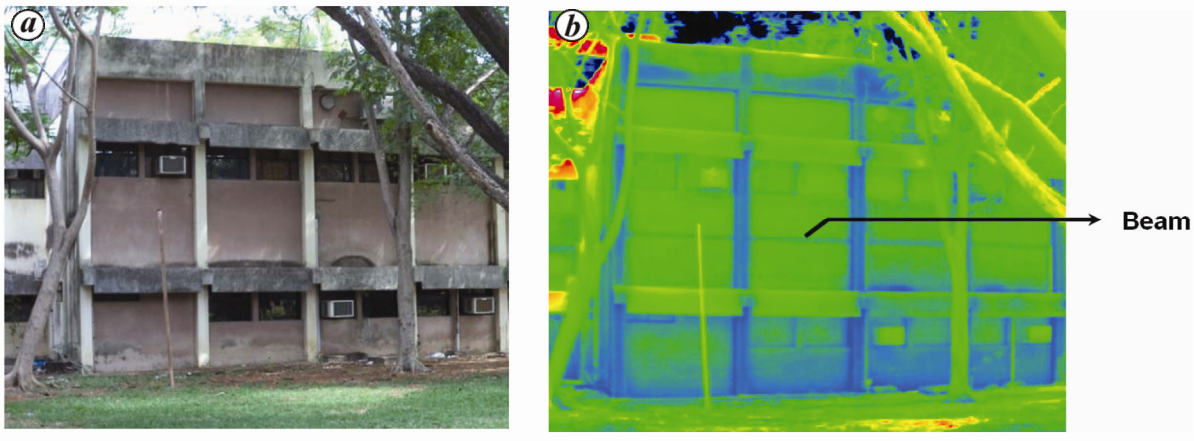

Figure 8. Structural element identification on structure TS4. ***a***, Test structure 4; ***b***, Thermogram.

evaluation using IRT. For the investigation, two test structures (TS5 and TS6) have been considered which include a two and three storeyed framed structure.

The proposed improved thermography technique involves the selection of the appropriate mother wavelet function, its number of vanishing points, and the number of levels of decomposition. After detailed study, it has been observed that the Daubechies wavelet function with four vanishing moments is effective in denoising thermograms. It has also been identified that signal decomposition up to fourth level needs to be performed to effectively improve the thermogram. For conducting the wavelet packet analysis, routines have been developed using Matlab®. One-dimensional wavelet packet analysis has been used in the present work. Denoising has been carried out along each line of the vertical axis (*Y*-axis)

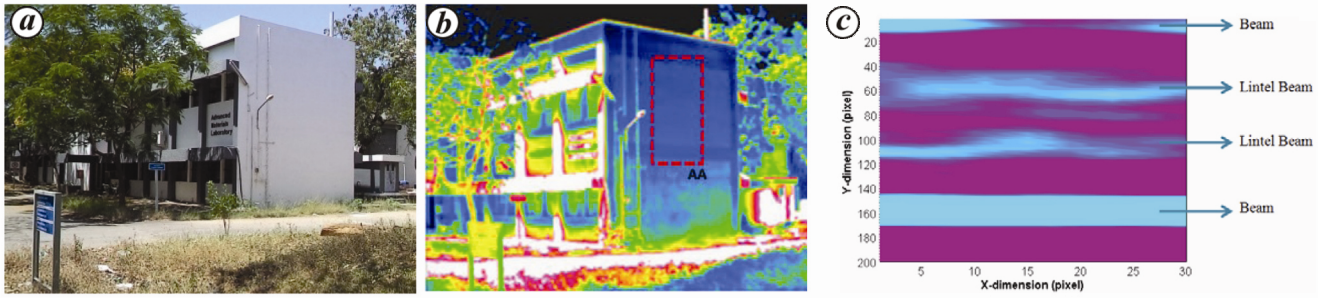

Figure 9. Identification of lintel beams using improved infrared thermography. ***a***, Test structure 5; ***b***, Thermogram, ***c***, Improved IRT results for region *AA* in Figure 9 *b*.

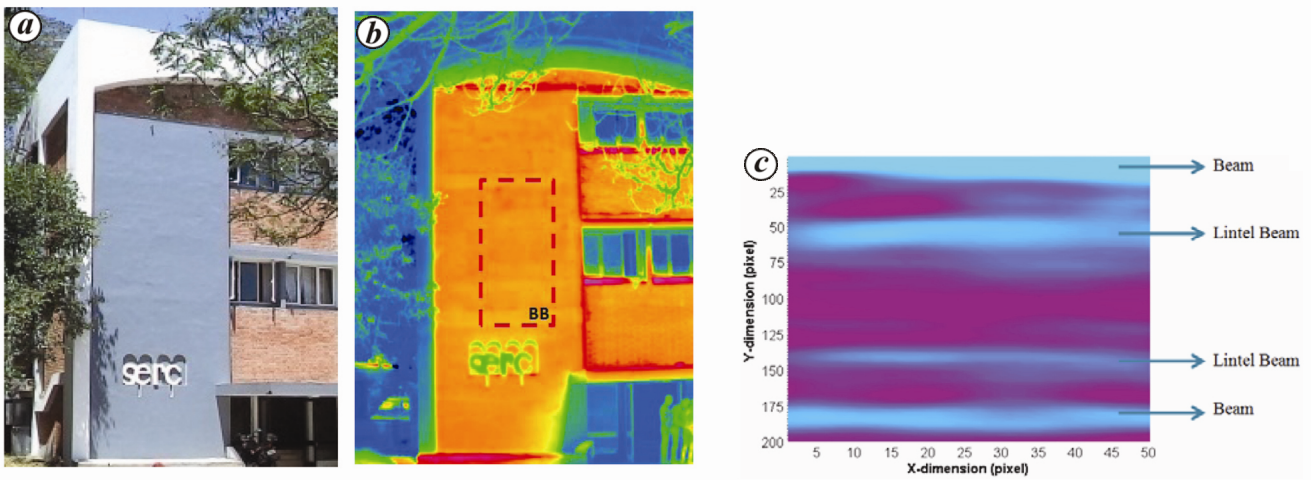

Figure 10. Investigation of a two-storey building wall. ***a***, Test structure 6; ***b***, Thermogram, ***c***, Improved IRT results for region *BB* in Figure 10 *b*.

Table 1. Estimation of the possible geometric dimensions from the infrared thermogram

	Difference (pixel)	Evaluated dimension (m)	Actual dimension (m)	Estimation error (%)
Test structure 5				
Ground floor roof beam	34	0.58	0.58	–
First floor roof beam	31	0.52882	0.58	8.82
First floor height	243	4.14529	3.86	7.39
Test structure 6				
Portico height	184	2.1	2.1	–
Portico thickness	25	0.28533	0.31	7.96
Ground floor height	322	3.675	3.8	3.29
First floor height	305	3.48098	3.635	4.24

alone. This is because the variation in the thermal gradient along the vertical axis reveals the main and lintel beams. Hence, to improve the thermograms, denoising has been carried out along the vertical axis alone.

A photograph of TS5 is shown in Figure 9 *a*. The thermogram obtained for the exterior frame shows the beams and columns clearly (Figure 9 *b*). However, the smaller RC members like lintel beams cannot be observed in the thermogram. The region AA as indicated in Figure 9 *b* has been selected for applying the wavelet packet analysis. This region has been selected to reduce wide variations in the temperature and thus facilitate in the effective analysis of the thermogram. The filtering analysis has been applied and the thermogram is improved to identify the lintel beams between the ground floor and first floor main beams. The improved thermogram is shown in Figure 9 *c*.

On similar lines, the sixth test structure (TS6) has been tested using IRT. A photograph of the test structure and

the thermogram are shown in Figure 10 *a* and *b* respectively. Here, the main beams are identifiable from the thermogram. The region *BB* indicated in Figure 10 *b* has been considered for the wavelet packet analysis. The improved thermogram is shown in Figure 10 *c*, wherein the lintel beams between the ground and first floor beams are identifiable. Thus, it can be observed that the results of the thermogram obtained using the IR cameras have been improved using signal processing techniques to enhance the non-destructive identification process.

Estimation of geometric dimensions using the thermogram

To further exploit the thermogram for more details, an attempt was made to evaluate the geometric dimensions from the thermogram. Towards this, the thermogram was converted into ASCII format, loaded into MATLAB® software and converted into pixel data. The pixel dataset contains RGB information at each pixel. Now, the pixel data corresponding to any one of the structural members was mapped to its actual geometric dimension. This mapping was then used to evaluate the dimension of other structural elements observed in the thermogram. The dimensions were compared with the actual values and the errors studied.

To conduct this study, TS5 and TS6 (shown in Figures 9 *a* and 10 *a* respectively) along with their thermograms (in Figures 9 *b* and 10 *b* respectively) are considered. To demonstrate the evaluation of the geometric dimensions, only the vertical dimensions were considered. Here, care was taken to compute the pixel information corresponding to a constant *X*-axis value. Thus, it was ensured that the dimension is measured along the vertical axis. However, any minor tilt of the structure in the thermogram image, that is present with respect to the vertical axis was not considered. It needs to be noted that this is also expected to contribute to the error in the evaluation of the dimensions. As the thermograms have been captured at acute angle to the transverse direction, the horizontal dimensions could not be evaluated. However, the procedure is obvious and the evaluation process could be extended to other directions if the thermogram was captured without any camera inclination.

To evaluate the vertical dimensions in TS5, the size of the ground floor roof beam was used for pixel mapping, i.e. the 34 pixels in the thermogram correspond to a beam size of 0.58 m. Now, the first floor roof beam size and first floor height were evaluated. Details of the evaluation are shown in Table 1. It has been observed that the dimensions could be evaluated with errors less than 9%. Similarly, in TS6 the portico height has been taken as reference, for mapping the pixel data. Then, the portico thickness, ground floor and first floor height were evaluated. Here too, it has been observed that the errors in estimation are less than 8%. Table 1 shows the actual and evaluated dimensions of TS6. Thus, it has been demonstrated that the thermogram could be used for evaluation of geometric dimensions also with more than 90% accuracy.

Conclusions

The present study focuses on applying the IRT technique to civil engineering structures. The initial part of the study focussed on identifying the beams and masonry walls using the IR thermogram. Four test structures were considered for the initial investigation. Results indicate that the IRT could be used to identify the RC and masonry members without ambiguity, under ambient conditions. However, when the same technique was extended to the RC framed structures, it was observed that the thermograms revealed lesser information. The expectations to differentiate between the RC and masonry elements were constrained as the lintel beams could not be identified. Hence, wavelet packet analysis was adopted to improve the thermograms. Two test structures were studied for demonstrating the need for improved post-processing. The wavelet packet analysis has been used to effectively reduce the noise in the thermograms and hence bring out the thermal gradients corresponding to the lintel beams. Thus, it has been demonstrated through this study that thermal gradients smudged in the noise could be brought out by the application of an appropriate and effective denoising technique. From the results it has been observed that the lintel beams could be identified in both the framed structures using improved thermography.

Later, mapping of pixels with actual geometry has been carried out to evaluate the geometric dimensions of structural members and floor heights from the thermogram images. Two test structures have been used for the study. It has been observed that the geometric dimensions could be evaluated with less than 9% error.

With continued research in this area, IRT will find applications in identifying concealed electric lines, water pipes, hot gas pipes in industries and many more in civil engineering structures. The encouraging results from this research work also provide confidence that the IRT technique can grow into a useful non-destructive testing method for evaluation of concrete and heritage structures in the future. The method would be of interest especially because of its non-contact nature.

1. Vreugdenburg, T. D., Willis, C. D., Mundy, L. and Hiller, J. E., A systematic review of elastography, electrical impedance scanning, and digital infrared thermography for breast cancer screening and diagnosis. *Breast Can. Res. Treatment*, 2013, **137**(3), 665–676.
2. Jadin, M. S. and Taib, S., Recent progress in diagnosing the reliability of electrical equipment by using infrared thermography. *Infrared Phys. Technol.*, 2012, **55**(4), 236–245.

3. Usamentiaga, R., Garcia, D. F, Molleda, J., Bulnes, F. G. and Orgeira, V. G., Temperature tracking system for sinter material in a rotatory cooler based on infrared thermography. In IEEE Proceedings of Industry Applications Society Annual Meeting, Lake Buena Vista, FL, 6–11 October 2013, pp. 1–8.
4. Zhang, Z., Bin, L. and Jiang, Y., Slag detection system based on infrared temperature measurement, *Optik – Int. J. Light Electron Opt.*, 2014, **125**(3), 1412–1416.
5. Carosena, M. and Cinzia, T., Nondestructive evaluation of carbon fiber reinforced polymers with ultrasonics and infrared thermography: an overview on historical steps and patents. *Rec. Patents Mater. Sci.*, 2012, **5**(1), 48–67.
6. Manohar, A. and Scalea, F. L., Defect detection in composite structures using lock-in infrared thermography, residual stress, thermomechanics and infrared imaging. *Hybrid Techn. Inverse Prob.*, In Proceedings of the Society for Experimental Mechanics Series 2014, vol. 8, pp. 135–141.
7. Yang, B., Huang, Y. and Cheng, L., Defect detection and evaluation of ultrasonic infrared thermography for aerospace CFRP composites. *Inf. Phys. Technol.*, 2013, **60**, 166–173.
8. Sakagami, T. and Kubo, S., Development of a new non-destructive testing technique for quantitative evaluations of delamination defects in concrete structures based on phase delay measurement using lock-in thermography. *Inf. Phys. Technol.*, 2002, **43**(3–5), 311–316.
9. Lai, W. L., Kou, S. C., Poon, C. S., Tsang, W. F. and Lai, C. C., Effects of elevated water temperatures on interfacial delaminations, failure modes and shear strength in externally-bonded CFRP-concrete beams using infrared thermography, gray-scale images and direct shear test. *Const. Build. Mater.*, 2009, **23**(10), 3152–3160.
10. Milovanovic, B. and Pecur, I. B., The role of infrared thermography in nondestrcutive testing of civil engineering structures. Matest 2011, In Proceedings/Krnic, Niksa (ed) – Zagreb, 2011.
11. Dumoulin, J., Ibos, L., Marchetti, M. and Mazioud, A., Detection of non-emergent defects in asphalt pavement samples by long pulse and pulse phase infrared thermography. *Eur. J. Environ. Civil Eng.*, 2011, **15**(4), 557–574.
12. Chiang, C.-H., Cheng, C.-C. and Hsu, K.-T., Inspection of deteriorated coastal embankments using radar, thermography, and impact-Echo. In *Nondestructive Test. Mater. Struct.*, RILEM Book Series, Springer Science and Business Media, 2013, **6**, 927–933.
13. Belattar, S., Rhazi, J. and Ballouti, A. E., Non-destructive testing by infrared thermography of the void and honeycomb type defect in the concrete. *Int. J. Microst. Mater. Prop.*, 2012, **7**(2–3), 235–253.
14. Carcangiu, S., Cannas, B., Concu, G. and Trulli, N., Modeling of active infrared thermography for defect detection in concrete structures. In Proceedings of the 2012 COMSOL Conference, Milan, 2012.
15. Minkina, W. and Dudzik, S., *Infrared Thermography: Errors and Uncertainties*, John Wiley, 2009, p. 212.
16. Mallat, S., *A Wavelet Tour of Signal Processing: The Sparse Way*, Academic Press, 2008, 3rd edn, p. 832.
17. Pathak, R. S., *The Wavelet Transform*, *Volume 4 of Atlantis Studies in Mathematics for Engineering and Science*, Atlantis Press, 2009, p. 191.
18. Addison, P. S., *The Illustrated Wavelet Transform Handbook: Introductory Theory and Applications in Science, Engineering, Medicine and Finance*, CRC Press, 2010, p. 368.
19. Sayood, K., *Introduction to Data Compression*, The Morgan Kaufmann Series in Multimedia Information and Systems, Morgan Kaufmann, USA, 4th edn., 2012.
20. Adeli, H. and Jiang, X., Dynamic fuzzy wavelet neural network model for structural system identification. *ASCE-J. Struct. Eng.*, 2006, **132**(1), 102–111.
21. Jiang, X. and Adeli, H., Dynamic fuzzy wavelet neuroemulator for non-linear control of irregular building structures. *Int. J. Numer. Meth. Eng.*, 2008, **74(7)**, 1045–1066.
22. Kareem, A., Gurley, K. and Kantor, J. C., Time-scale analysis of nonstationary processes utilizing wavelet transforms, In Proceedings of the 6th International Conference on Structural Safety and Reliability, Innsbruck, Austria, Balkema Publishers, Amsterdam, The Netherlands, 1993.
23. Amiri, G., Abdolahi Rad, G. and Khorasani, A., Generation of near-field artificial ground motions compatible with median predicted spectra using PSO-based neural network and wavelet analysis. *Comput.-Aided Civ. Infrastruct. Eng.*, 2012, **27**(9), 711–730.
24. Zhu, X. Q. and Law, S. S., Wavelet-based crack identification of bridge beam from operational deflection time history. *Int. J. Solids Struct.*, 2006, **43**(7–8), 2299–2317.
25. Adeli, H. and Kim, H., *Wavelet-Based Vibration Control of Smart Buildings and Bridges*, CRC Press, Taylor & Francis, 2009, p. 219.
26. Adeli, H. and Jiang, X., *Intelligent Infrastructure: Neural Networks, Wavelets, and Chaos Theory for Intelligent Transportation Systems and Smart Structures*, Taylor & Francis Group, 2009, p. 420.
27. Amini, F., Khanmohamadi Hazaveh, N. and Abdolahi Rad, A., Wavelet PSO-based LQR algorithm for optimal structural control using active tuned mass dampers. *Comput.-Aided Civ. Infrastruct. Eng.*, 2013, **28**(7), 542–557.
28. Sivasubramanian, K. and Umesha, P. K., Damage identification in beams using discrete wavelet transforms. *Int. J. Civ. Struct. Eng.*, 2012, **2**(3), 950–969.
29. Sivasubramanian, K. and Umesha, P. K., Wavelet transform for damage identification in continuous beams. *Int. J. Appl. Sci. Eng. Res.*, 2013, **2**(3), 294–306.
30. Sivasubramanian, K. and Umesha, P. K., Multiple damage identification in beams using continuous wavelet transforms, *Asian J. Civ. Eng. (BHRC)*, 2014, **15**(4), 605–634.
31. Umesha, P. K., Ravichandran, R. and Sivasubramanian, K., Crack detection and quantification in beams using wavelets. *Comput.-Aid. Civ. Infrastruct. Eng.*, 2009, **24**(8), 593–607.
32. Qiao, L., Esmaeily, A. and Melhem, H. G., Signal pattern recognition for damage diagnosis in structures. *Comput.-Aid. Civ. Infrastruct. Eng.*, 2012, **27**(9), 699–710.
33. Xiang, J. and Liang, M., Wavelet-based detection of beam cracks using modal shape and frequency measurements. *Comput.-Aid. Civ. Infrastruct. Eng.*, 2012, **27**(6), 439–454.
34. Jiang, X., Ma, Z. J. and Ren, W. X., Crack detection from the slope of the mode shape using complex continuous wavelet transform. *Comput.-Aid. Civ. Infrastruct. Eng.*, 2012, **27**(3), 187–201.
35. Epasto, G., Proverbio, E. and Venturi, V., Evaluation of fire-damaged concrete using impact-echo method. *Mater. Struct.*, 2010, **43**, 235–245; doi: 10.1617/s11527-009-9484-0.

ACKNOWLEDGEMENTS. We thank the Director, CSIR-SERC, Chennai for persmission to publish this paper and Innovation Complex at CSIR-SERC, for providing the infrared thermography equipment for conducting this work.

Received 16 May 2014; revised accepted 22 November 2014